Degenerate Ising model for atomistic simulation of crystal-melt interfaces

D. Schebarchov,[1] T. P. Schulze,[2] and S. C. Hendy[1]
[1)] *The MacDiarmid Institute for Advanced Materials and Nanotechnology, School of Chemical and Physical Sciences, Victoria University of Wellington, Wellington 6140, New Zealand*
[2)] *Department of Mathematics, University of Tennessee, Knoxville, TN 37996-1300, USA*

(Dated: 6 November 2013)

One of the simplest microscopic models for a thermally driven first-order phase transition is an Ising-type lattice system with nearest-neighbour interactions, an external field and a *degeneracy* parameter. The underlying lattice and the interaction coupling constant control the anisotropic energy of the phase boundary, the field strength represents the bulk latent heat, and the degeneracy quantifies the difference in communal entropy between the two phases. We evolve this minimal model by applying rejection-free canonical and microcanonical Monte Carlo algorithms, and we obtain caloric curves and heat capacity plots for square (2D) and face-centred cubic (3D) lattices with periodic boundary conditions. Since the model admits precise adjustment of bulk latent heat and communal entropy, neither of which affect the interface properties, we are able to tune the crystal nucleation barriers at a fixed degree of undercooling and verify a dimension-dependent scaling expected from classical nucleation theory. We also analyse the equilibrium crystal-melt coexistence in the microcanonical ensemble, where we detect negative specific heat capacities and find that this phenomenon is more pronounced when the interface is the dominant contributor to the total entropy. The negative branch of the heat capacity appears smooth only when the equilibrium interface-area-to-volume ratio is not constant but varies smoothly with the excitation energy. Finally, we simulate microcanonical crystal nucleation and subsequent relaxation to an equilibrium Wulff shape, demonstrating the model's utility in tracking crystal-melt interfaces at the atomistic level.

I. INTRODUCTION

Melting and crystallisation are common examples of a first-order phase transition, and manipulating these processes is an important aspect of materials science.[1] The consequent demand for predictive capability has motivated the development of numerous theoretical methods, with continuum models at one end of the spectrum, and molecular dynamics (MD) simulations at the other extreme. MD provides a fully atomistic description of multi-phase systems, but the associated computational cost restricts the approach to relatively small length- and time-scales, making it difficult to simulate rare events (such as phase nucleation). This restriction does not apply to continuum models, but there the difficulty lies in formulating a description of the phase boundary, and any continuum model inevitably fails to provide a meaningful picture of the microscopic mechanisms operating at the nanometre scale. In order to reach a suitable compromise, it is desirable to pursue a mesoscopic approach with an appropriate level of coarse-graining. Phase field crystal (PFC)[2] modelling is one possible way forward, but it still does not offer an intuitive microscopic picture. In the present contribution we outline an alternative approach based on lattice Monte Carlo (MC), which admits a highly intuitive microscopic description of the interface structure and kinetics, and it allows for precise adjustment of the volumetric contribution to the relevant thermodynamic potential, facilitating the simulation of phase nucleation.

Lattice models have played an important role in shaping the current understanding of crystal growth.[3] Kinetic lattice MC models have also been recognised as an effective method for simulating microscopic dynamics at long time-scales, thus filling the wide gap between what can be accomplished with continuum models and MD studies. Examples where this approach has proven effective include the growth of thin films in chemical vapour deposition,[4] the relaxation of nanoscale atomic clusters in vacuum,[5] the growth of dendrites in a dilute solution,[6] etc. In many of these applications the objective is to track the interface between a condensed phase and a dilute (gas-like) environment or vacuum, in which case the atomistic interpretation of a two-component lattice system is clear: an occupied lattice site represents an atom, and a vacant site represents empty space. Modelling the solidification of a pure melt, however, requires the identification of an interface between two condensed phases, and it does not necessarily make sense to classify individual atoms as solid or liquid at such a boundary. Still, in MD simulations the two phases can be fairly well distinguished by an appropriate *local* order parameter (see Fig. 1). A two-state lattice model can be viewed as describing the behaviour of such an order parameter, whose globally-averaged value may fluctuate. Note that the assignment of liquid atoms to a fixed lattice is an approximation: many melt-specific characteristics will be lost as a result; but some of the lost features that are necessary for the description of the phase boundary can potentially be reintroduced *via* additional (preferably meaningful) parameters.

A simple and intuitive model for cohesion in a two-component lattice system is the binary alloy model.[9] It is based on the assumption that only the adjacent sites can interact with each other, and that these interactions can

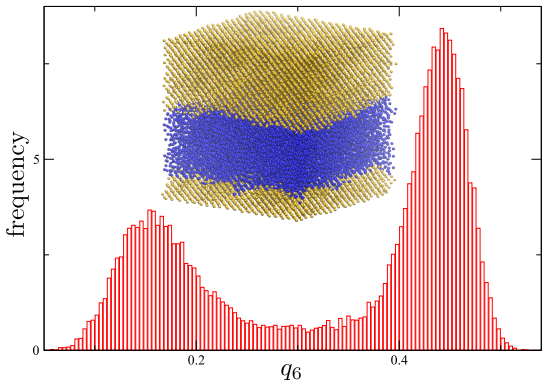

FIG. 1. Distribution of instantaneous values of the Steinhardt q_6 local order parameter,[7] refined using the scheme of Lechner and Dellago,[8] in a single configuration from a microcanonical MD simulation of coexisting (bulk) Lennard-Jones system containing 32000 atoms with periodic boundary conditions. The distribution is clearly bimodal, so we can characterise atoms with $q_6 > 0.3$ as ordered (face-centred cubic) and disordered otherwise. The inset illustrates the configuration with ordered atoms coloured in gold and disordered in blue.

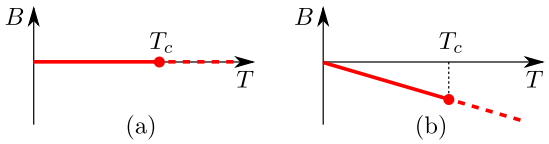

FIG. 2. The BT phase diagram for (a) the ferromagnetic Ising model and (b) the degenerate variant with $\delta > 0$ carried by one of the two atomic states. The red line represents a phase boundary: crossing the solid portion constitutes a first-order phase transition, while the dashed portion is associated with a smooth transition. The dot at $T = T_c$ represents a critical point: a second-order transition will occur when the point is passed while traversing *along* the phase boundary. The slope of the boundary is $-\frac{1}{2}k_B \ln \delta$, and the value of T_c is independent of B or δ.

be characterised by a fixed energy parameter. The total potential energy then becomes a weighted sum of nearest-neighbour "bonds", with only three distinct bond types. This energy function can be recast in the more familiar form of a spin-half Ising Hamiltonian with a coupling constant J and an external field of magnitude B. The statistical mechanics of spin-half Ising systems is relatively well understood:[10] in the absence of an external field ($B = 0$), on a lattice with coordination number greater than three, there is a *temperature*-driven *second*-order transition at a lattice-specific temperature T_c. There is also a *field*-driven *first*-order transition at $B_f = 0$ for all $T < T_c$ (see Fig. 1a). In order to study *temperature*-driven *first*-order transitions, Harris[11] has modified the Ising model so that the first-order transition occurs at a particular temperature $T_f < T_c$ and $B_f \neq 0$. Harris's modification relies on just one additional parameter, $\delta > 0$ — akin to *fugacity* in the lattice gas model with non-conserved number of particles[9,12] — which adjusts the relative weightings of the two possible atomic states in the partition function. This reweighting effectively introduces degenerate states into the system, and δ represents the degeneracy ratio of one atomic state to the other. It is also meaningful to think of δ as the difference in communal entropy between the two phases, and its value fully determines the slope of the phase boundary in the BT phase diagram (see Fig. 2b). This key feature extends the binary alloy model to heterogeneous systems composed of two energetically- and entropically-distinct condensed phases. Since the relative fraction of constituent phases can fluctuate, the resultant model is perhaps better described as a *reactive* binary alloy.

The aim of this work is to combine Harris's degenerate Ising model with Ray's microcanonical Monte Carlo approach[12] and study equilibrium crystal-melt coexistence. Recall that a crystal-melt boundary is inherently unstable in the canonical ensemble at fixed temperature, because the interface free energy is usually positive, and the system can always lower its total free energy by adopting a homogeneous state (i.e. fully solid or fully liquid). In the microcanonical ensemble it is the total energy and not the temperature that is fixed, with the equilibrium behaviour of a system now dictated by the principle of maximum entropy, and when passing through the solid-liquid transition the solid and liquid phases can be forces to coexist indefinitely under certain conditions. Constraining the total energy makes it possible to study the equilibrium properties of the phase boundary, and it also admits the possibility of direct comparison with MD. Our implementation of microcanonical Monte Carlo is based on the work of Ray,[12] which differs from the approach taken by Harris *et al.*[11,13,14], who used Creutz's N-demon algorithm.[15] We found that the simplest form of Creutz's algorithm (with just one demon) exhibits pronounced and somewhat inconvenient artefacts due to the discrete nature of the potential energy landscape. These discrete effects are rendered negligible in Ray's approach, which is actually more natural than Creutz's for classical N-particle systems and is equally straightforward to implement.

The format of the paper is as follows. In Sec. II we formulate the degenerate Ising model and the rejection-free MC method for simulations at constant temperature. In Sec. III we analyse the model's canonical behaviour on a square lattice. We show how the degeneracy parameter admits precise control of the free energy barriers associated with the minority phase nucleation, and we exploit this feature to test a dimension-dependent scaling expected from classical nucleation theory. In Sec. IV we outline Ray's[12] approach to microcanonical MC and use it to perform constant-energy simulations on square (2D) and fcc (3D) lattices. We focus on the equilibrium crystal-melt coexistence and discuss the occurrence of negative heat capacities. We also simulate microcnaonical nucleation and subsequent relaxation to an equilibrium Wulff shape. Sec. V serves as a brief summary.

II. DEGENERATE ISING MODEL

A. Mapping of a binary alloy to an Ising spin system

Consider a d-dimensional periodic lattice with coordination number z and assume that all the potential energy is stored in the nearest-neighbour bonds. Each lattice site can be either solid (represented by $\downarrow$ to indicate that it is the lower energy state) or liquid ($\uparrow$), which calls for three distinct bond types: solid-solid ($\downarrow\downarrow$), solid-liquid ($\downarrow\uparrow$) and liquid-liquid ($\uparrow\uparrow$); and the corresponding energies will be specified by (positive) parameters $\varepsilon_{\downarrow\downarrow}$, $\varepsilon_{\downarrow\uparrow}$ and $\varepsilon_{\uparrow\uparrow}$. The total potential is then

$$\mathcal{U} = -\varepsilon_{\downarrow\downarrow}N_{\downarrow\downarrow} - \varepsilon_{\uparrow\uparrow}N_{\uparrow\uparrow} - \varepsilon_{\downarrow\uparrow}N_{\downarrow\uparrow}, \tag{1}$$

where $N_{\downarrow\downarrow}$, $N_{\downarrow\uparrow}$ and $N_{\uparrow\uparrow}$ are the bond counts that can vary from state to state. Equation (1) is often referred to as the binary alloy or bond-counting model. Assuming the periodic lattice has no vacancies, the total site- and bond counts will respect the following relations: $N_\downarrow + N_\uparrow = N$, $N_{\uparrow\uparrow} = zN/2 - N_{\downarrow\uparrow} - N_{\downarrow\downarrow}$, and $N_{\downarrow\uparrow} = zN_\downarrow - 2N_{\downarrow\downarrow} = zN_\uparrow - 2N_{\uparrow\uparrow}$; which allow us to express (1) in terms of just two independent variables, say $N_\downarrow$ and $N_{\downarrow\downarrow}$:

$$\mathcal{U} = -(\varepsilon_{\downarrow\downarrow}+\varepsilon_{\uparrow\uparrow}-2\varepsilon_{\downarrow\uparrow})N_{\downarrow\downarrow} - (\varepsilon_{\downarrow\uparrow}-\varepsilon_{\downarrow\downarrow})zN_\downarrow - \varepsilon_{\uparrow\uparrow}\frac{zN}{2}. \tag{2}$$

To connect with the Ising model, we now represent the state of each site by an integer σ, which takes a value of -1 for $\downarrow$ and $+1$ for $\uparrow$, so the entire configuration space is now described by $\boldsymbol{\sigma} = \{\sigma_n \in \{\pm 1\}\}_{n=1}^N$. In this representation

$$N_\downarrow = \frac{1}{2}\sum_n (1-\sigma_n) \quad \text{and} \quad N_{\downarrow\downarrow} = \frac{1}{4}\sum_{\langle m,n\rangle} (1-\sigma_m)(1-\sigma_n),$$

where $\langle m,n\rangle$ denotes the set of all distinct nearest-neighbour pairs (without double counting). After substituting these expressions for $N_{\downarrow\downarrow}$ and $N_\downarrow$ into (2), some algebraic manipulation yields the Ising-like form:

$$\mathcal{U}(\boldsymbol{\sigma}) = -B\sum_n \sigma_n - J\sum_{\langle m,n\rangle} \sigma_m\sigma_n + C, \tag{3}$$

where, in the context of ferromagnets, the parameter $B = z(\varepsilon_{\uparrow\uparrow} - \varepsilon_{\downarrow\downarrow})/4$ models the effect of an external field and $J = (\varepsilon_{\downarrow\downarrow}+\varepsilon_{\uparrow\uparrow}-2\varepsilon_{\downarrow\uparrow})/4$ is a coupling constant characterising the interaction between neighbouring sites. The additive constant $C = zN(\varepsilon_{\downarrow\downarrow} + \varepsilon_{\uparrow\uparrow} + 2\varepsilon_{\downarrow\uparrow})/8$ merely shifts the energy scale, so the underlying statistical mechanics is the same as in the traditional spin-half Ising model. For future reference we also note the inverse mapping:

$$\left.\begin{aligned} \varepsilon_{\downarrow\downarrow} &= J - 2B/z + 2C/(zN), \\ \varepsilon_{\uparrow\uparrow} &= J + 2B/z + 2C/(zN), \\ \varepsilon_{\downarrow\uparrow} &= -J + 2C/(zN). \end{aligned}\right\} \tag{4}$$

B. Canonical Monte Carlo

The equilibrium behaviour of the Ising model under particular physical constraints is usually studied by sampling the appropriate ensemble using MC. This procedure usually takes the form of a Markov chain with transition probabilities (i.e. normalised *rates*) between states satisfying a principle of detailed balance:

$$\rho(\boldsymbol{\sigma}_i)P_{ij} = \rho(\boldsymbol{\sigma}_j)P_{ji}. \tag{5}$$

Here P is the Markov transition matrix such that $P_{ij} \equiv P(\boldsymbol{\sigma}_i \to \boldsymbol{\sigma}_j)$ is the probability of traversing from state $\boldsymbol{\sigma}_i$ to state $\boldsymbol{\sigma}_j$, P_{ji} is the probability of the reverse transition (i.e. $\boldsymbol{\sigma}_j \to \boldsymbol{\sigma}_i$), and $\rho(\boldsymbol{\sigma})$ is the ensemble-specific (equilibrium) probability distribution. Note that the Markov matrix must satisfy $\sum_j P_{ij} = 1$, which is enforced by normalising the transition rates r_{ij}: $P_{ij} = r_{ij}/\sum_j r_{ij}$. In practice, only a relatively small number of transitions are allowed, with most of the rates set to zero. For example, it is common to only allow transitions that flip the sign of a single spin component σ_n. (In the crystal-melt system this is to be interpreted as a single atom changing phase, as determined by the local order parameter.) When choosing which transitions to allow, one must be careful to assure ergodicity: it must be possible for a sequence of transitions to navigate between any two possible states. Even with this choice made, detailed balance does not come close to prescribing unique rates. The most common choice is due to Metropolis *et al.*,[16] where transitions correspond to individual spins flipping with the rates

$$r_{ij} = \min\{1, \rho(\boldsymbol{\sigma}_j)/\rho(\boldsymbol{\sigma}_i)\}, \tag{6}$$

where j runs over all states $\boldsymbol{\sigma}_j$ that differ from $\boldsymbol{\sigma}_i$ at a single lattice site. In the Metropolis scheme all flips are attempted at a *uniform* rate and accepted with probability equal to r_{ij}. In effect, this also defines null moves by assigning a rejection rate $1-r_{ij}$ to each of the attempted flip moves. Collectively, the rejected moves contribute to a rate,

$$\tilde{r}_{ii} = 1 - \sum_j r_{ij}, \tag{7}$$

to do nothing on a given MC time step. The sum of the rates for any state i is then constant:

$$\tilde{r}_{ii} + \sum_j r_{ij} = N,$$

so that the normalized probabilities satisfy (5) with ρ equal to the Boltzmann distribution.

When the computational cost of the rejected moves is high, an alternative algorithm, due to Bortz, Kalos and Lebowitz (BKL)[17], is to discard the rejection moves and always perform a flip with the rates (6). This corresponds

to simulating a continuous time Markov process, where the detailed balance condition now takes the form

$$\rho(\boldsymbol{\sigma}_i) r_{ij} = \rho(\boldsymbol{\sigma}_j) r_{ji}, \tag{8}$$

and one must associate nonuniform time-intervals between jumps governed by a Poisson process with a total rate $R_i = \sum_j r_{ij}$ for jumping out of state i. This modification once again allows the detailed balance condition to be satisfied by the Boltzmann distribution.

The Boltzmann distribution models a system coupled to a heat reservoir at constant temperature T — a situation described by the canonical ensemble. Each state $\boldsymbol{\sigma}$ is weighted by a Boltzmann factor $\exp(-\beta\mathcal{U}(\boldsymbol{\sigma}))$, with $\beta \equiv (k_B T)^{-1}$ denoting the reciprocal of the thermodynamic temperature, and the distribution function is:

$$\rho_T(\boldsymbol{\sigma}) = Z^{-1} \exp(-\beta\mathcal{U}(\boldsymbol{\sigma})), \tag{9}$$

where Z is the canonical partition function. Note that, when obtaining canonical ensemble averages, the kinetic part ($\mathcal{K}$) of a Hamiltonian separates and integrates to the same constant for every Boltzmann factor. Hence, the parameter β should be interpreted as a fixed constraint that defines the ensemble. In the microcanonical ensemble for isolated systems, however, it becomes necessary to introduce additional degree(s) of freedom to mimic the fluctuating kinetic contribution in the Hamiltonian.

C. Harris's degeneracy parameter

For reasons that have already been stated in Sec. I, Harris[11] has modified the ferromagnetic Ising model by introducing degenerate states into the model, which effectively amounts to using the grand canonical ensemble with the following probability distribution:

$$\begin{aligned} \tilde{\rho}_T(\boldsymbol{\sigma}) &= \widetilde{Z}^{-1} \delta^{N_\uparrow(\boldsymbol{\sigma})} \exp\left(-\beta\mathcal{U}(\boldsymbol{\sigma})\right) \\ &= \widetilde{Z}^{-1} \exp\left(-\beta\left\{\mathcal{U}(\boldsymbol{\sigma}) - N_\uparrow(\boldsymbol{\sigma}) k_B T \ln\delta\right\}\right) \end{aligned} \tag{10}$$

where $\delta > 0$ is a parameter introduced to act as an additional weighting factor for the liquid state, $N_\uparrow(\boldsymbol{\sigma}) = \frac{1}{2}\sum_n(\sigma_n + 1)$ is the number of "liquid" atoms (i.e. spins with $\sigma = +1$) in state $\boldsymbol{\sigma}$, and $\widetilde{Z}$ is what appears to be the grand canonical partition function:

$$\widetilde{Z} = \sum_i \delta^{N_\uparrow(\boldsymbol{\sigma}_i)} \exp\left(-\beta\mathcal{U}(\boldsymbol{\sigma}_i)\right). \tag{11}$$

Note that δ would normally be called *fugacity* in the grand canonical sense,[9,18] but here we interpret it as a parameter that controls the communal entropy of the liquid phase, allowing us to compensate for the phase space that has been lost as a consequence of liquid atoms being restricted to a lattice (on par with the solid). Hence, we refer to δ as the liquid *degeneracy* or *multiplicity* parameter, and we set $\delta > 1$ to endow the liquid with more entropy. With this simple modification each Boltzmann factor now contains an effective potential

$$\begin{aligned} \widetilde{\mathcal{U}}(\boldsymbol{\sigma}) &\equiv \mathcal{U}(\boldsymbol{\sigma}) - N_l k_B T \ln\delta \\ &= -\left(B + \frac{1}{2} k_B T \ln\delta\right) \sum_i \sigma_i - J \sum_{\langle i,j\rangle} \sigma_i \sigma_j \\ &\quad -\frac{1}{2} N k_B T \ln\delta \end{aligned}$$

where the last term is a constant that has little effect on the underlying statistical mechanics and (in most cases) can be ignored. A desirable feature in $\widetilde{\mathcal{U}}$ is the effective field

$$B_{eff} \equiv B + \frac{1}{2} k_B T \ln\delta \tag{12}$$

passing through zero at a particular temperature T_f:

$$T_f = \frac{-2B}{k_B \ln\delta}, \tag{13}$$

which is positive when B and $\ln\delta$ have opposite signs. Note that $-2B = z(\varepsilon_{\downarrow\downarrow} - \varepsilon_{\uparrow\uparrow})/2$ can be thought of as the latent heat and $k_B \ln\delta$ as the entropy change (both per particle) during melting; so (13) is suggestively reminiscent of the thermodynamic relationship between the melting temperature (T_m), latent heat (L) and entropy change (ΔS): $T_m = L/\Delta S$. According to Harris,[11] if B and δ are specified so that $0 < T_f < T_c$, the modified Ising model will go through a first-order phase transition at $T = T_f$, as was already indicated in Fig. 2b. In Sec. III we will verify this temperature-driven first-order transition and analyse its features by Monte Carlo simulation, which will require the use of a modified set of rates:

$$\tilde{r}_{ij} = \begin{cases} \min\{1, \rho_T(\boldsymbol{\sigma}_j)/\rho_T(\boldsymbol{\sigma}_i)\} & \text{if } \sigma_n^i = -1, \\ \delta^{-1}\min\{1, \rho_T(\boldsymbol{\sigma}_j)/\rho_T(\boldsymbol{\sigma}_i)\} & \text{if } \sigma_n^i = +1, \end{cases} \tag{14}$$

where $\rho_T(\boldsymbol{\sigma})$ is the canonical (Boltzmann) distribution given in (9). With these rates, the average number of transitions with $\sigma_n = +1 \;\mapsto\; \sigma_n = -1$ is now a fraction $f = (\delta - 1)/\delta$ of that in (6).

D. Alternative formulations and links to other models

Before discussing simulated results, it is worthwhile commenting on how the degenerate Ising model relates to other better-known lattice models. Firstly, Griffiths[19] has pointed out that $\delta = 2$ corresponds to a special case of the spin-one Ising system (often referred to as the Blume-Emery-Griffiths model[20]). Extension to integer $\delta > 2$ can also be formulated somewhat analogously to the q-state Potts model,[21] with the state of each lattice site represented by $s_n \in \{-1, 1, 2, \ldots, q-1\}$ and the energy given by

$$\mathcal{U}_P = -J \sum_{\langle n,m\rangle} \mathrm{sgn}(s_n)\,\mathrm{sgn}(s_m) - B \sum_n \mathrm{sgn}(s_n).$$

Here the signum (sgn) function makes all positive states degenerate with effective $\delta = q - 1$. Generalization to rational values of δ can be achieved by allowing more negative states, i.e. $s_n \in \{-p, \ldots, -1, 1, \ldots, q\}$ so that $\delta = q/p$. Inclusion of all real numbers may be possible through an XY-like model, where the state of each lattice site is represented by a continuous variable. However, Harris's approach of manipulating the relative weighting of only two Ising-like spin states *via* a single degeneracy parameter is more convenient.

Also, recall that Harris's δ gives rise to a temperature-dependent *effective* external field, which is precisely what Stevenson *et al.*[22] have introduced in their Ising-like model for glass forming liquids. However, in the context of two-phase systems, the notion of the degeneracy parameter is more meaningful than an effective field: $1/(1+\delta)$ and $\delta/(1+\delta)$ represent the fractions of total phase-space volume associated with the "solid" and "liquid" states, respectively. These fractions may be inferred from a more accurate description of the underlying energy landscape.

III. CANONICAL SIMULATIONS

A. Square lattice (2D)

We now discuss our results from canonical MC simulations on a square lattice. For this discussion it is convenient to adopt the following dimensionless quantities: $T^* \equiv k_B T/J$, $B^* \equiv B/J$ and $E^* \equiv E/NJ$, where E represents any form of energy (potential or kinetic). The datasets in Fig. 3 were obtained by annealing the system, initially in the ground state, from $T^* = 1.5$ to $T^* = 2.7$ or above, and then back to $T^* = 1.5$. For each annealing cycle the temperature was ramped in increments of 0.02. At each increment the system was first equilibrated for 10^4 MC steps, with one step defined by the number of attempted spin flips matching the total number of spins (10^4 for the 100×100 system); and averages were accumulated over another 10^4 MC steps, with just one contribution to the average from each step after its final spin-flip attempt. The canonical heat capacities (C_T) were calculated using the fluctuation formula

$$C_T = \left(\langle \mathcal{U}^2 \rangle - \langle \mathcal{U} \rangle^2\right) / (k_B T^2), \qquad (15)$$

and the corresponding dimensionless quantity is $C_T^* \equiv C_T/Nk_B$.

The C_T^* and net magnetization (M) plots in Fig. 3 for the case where $B^* = 0$ and $\delta = 1$ clearly exhibit the expected ferromagnetic transition near $T^* = 2.269$. The corresponding caloric curve (U^* versus T^*) shows no signs of a discontinuity, consistent with the transition being second-order. Setting $B^* = -1$ and $\delta = 3$, on the other hand, eliminates all signs of a transition at $T^* = 2.269$, and instead introduces a transition near the temperature $T_f^* = 1.82$ predicted by (13). Clear discontinuities in the corresponding caloric curves and noticeable

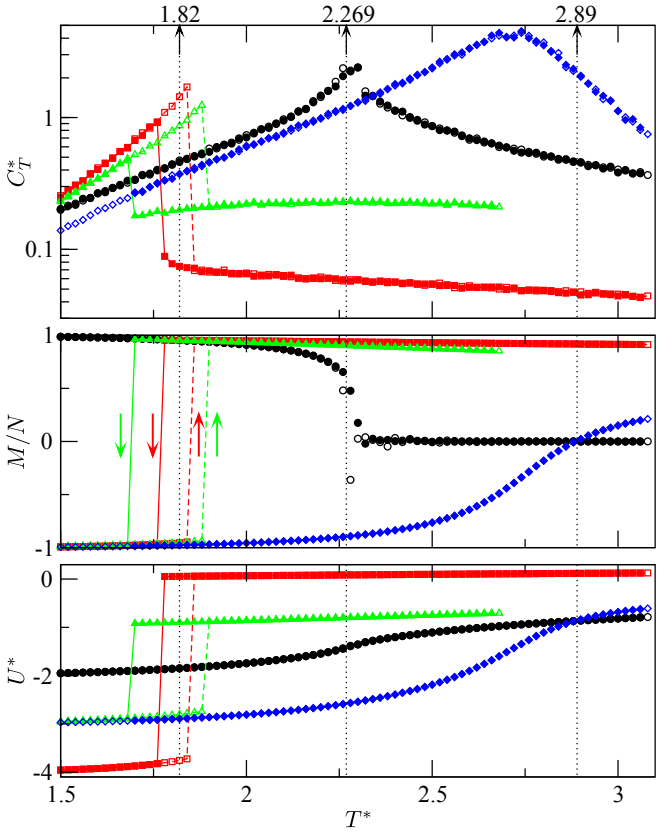

FIG. 3. Dimensionless specific heat (C_T^*), net magnetization (M/N) and potential (U^*) for the canonical degenerate Ising model on 100×100 square lattice. Note that the C_T^* axis has logarithmic scale. Hollow symbols correspond to the heating stage and filled symbols correspond to the cooling stage of the annealing cycle. The black circles ($B^* = 0$ and $\delta = 1$) show the second-order phase transition near $T_c^* = 2.269$. For red squares ($B^* = -2$, $\delta = 9$) and green triangles ($B^* = -1$, $\delta = 3$) the transition temperature predicted by (13) is $T_f^* = 1.82 < T_c^*$, whereas for blue diamonds ($B^* = -1$, $\delta = 2$) we have $T_f^* = 2.89 > T_c^*$.

hysteresis verify that the transition is first-order. Note that halving the temperature ramping rate had no significant effect on the hysteresis, indicating that the present rate was sufficient to allow the system to relax. Changing the value of B^* from -1 to -2 and δ from 3 to 9, while keeping $T_f^* = 1.82$ constant, leads to a less pronounced hysteresis and increases the size of the energy jump in the caloric curves (i.e. the latent heat). Finally, for $B^* = -1$ and $\delta = 2$ the net magnetization smoothly passes through zero at $T_f^* = 2.89 > T_c^*$, as anticipated; and the dimensionless heat capacity C^* peaks at around 2.7. The position and shape of this peak appears to be independent of system size, which indicates that it is not an artefact of periodic boundary conditions, but rather a feature that is possibly a remnant of the first- and second-order transitions.

B. Application of classical nucleation theory

The observed change in hysteresis at fixed $T_f^* = 1.82$ for two different combinations of B and δ (see Fig. 3) can be rationalised using classical nucleation theory. The formation of a minority-phase nucleus of d-dimensional "volume" $V \in \mathbb{R}^d$ and interface "area" $A \in \mathbb{R}^{d-1}$ will change the total free energy of the system by $\Delta F = V\Delta f + A\gamma$, where Δf is the contribution that scales with "volume" and $\gamma > 0$ scales with "area". The difference in scaling gives rise to a critical nucleus size and a corresponding energy difference

$$\Delta F^\dagger = \alpha_d \gamma^d (\Delta f)^{1-d}, \tag{16}$$

where α_d is a geometric factor whose sign changes with dimension: $\alpha = 16\pi/3$ for a sphere in $\mathbb{R}^3$, and $\alpha = -\pi$ for a circle in $\mathbb{R}^2$. Note that $\Delta F^\dagger > 0$ when $\Delta f < 0$, and it represents a barrier that must be surmounted in order to allow a nucleus to grow and form the new thermodynamically stable phase. From (16) it is clear that increasing the magnitude of Δf at fixed γ will reduce the magnitude of $\Delta F^\dagger$, which will make it easier for the new phase to nucleate and thus diminish the propensity for undercooling and overheating. This change can also render any manifestation of a hysteresis less pronounced.

In Harris's model, in the "dilute" regime (i.e. minimal phase intermixing) at temperatures well below T_c, the magnitude of the volumetric contribution to ΔF is twice the effective field defined in (12): $\Delta f_\pm \simeq \pm(2B + k_B T \ln\delta)$, where the minus sign is to be used when the solid ($\sigma = -1$) is the nucleating minority phase. It is also clear that γ should *not* depend on B or δ, because these two parameters are completely decoupled from interphase interactions (i.e. J or $\varepsilon_{\downarrow\uparrow}$). From this reasoning it follows that increasing B and δ at fixed T_f (and T) should raise the magnitude of Δf in a predictable manner, but have little or no effect on γ. The nucleation energy barrier in (16) is then expected to become smaller, which is consistent with the diminishing hysteresis in Fig. 3.

A large body of work[23] has already been done to asses the applicability of classical nucleation theory to Ising systems. Here we shall only briefly demonstrate how in the degenerate Ising system the average lifetime of a metastable liquid ($\sigma = +1$) can be adjusted at a fixed degree of undercooling. Recall that the rate I of crystal ($\sigma = -1$) nucleation is related to $\Delta F^\dagger$ via[24]

$$I = I_0 \exp\left(-\frac{\Delta F^\dagger}{k_B T}\right) = I_0 \exp\left(-\frac{\alpha_d \gamma^d}{(\Delta f)^{d-1} k_B T}\right),$$

where I_0 a prefactor with appropriate units, and it may weakly vary with temperature. As was already explained, we can adjust $\Delta f = -(2B + k_B T \ln\delta)$ at fixed T, T_f and γ, and then count the average number of MC steps (N_{MCS}) required for a nucleation event to occur. Since the cumulative number of MC steps (N_{MCS}) taken by the BKL algorithm becomes proportional to cumulative physical time (t_w) in the long run, so that

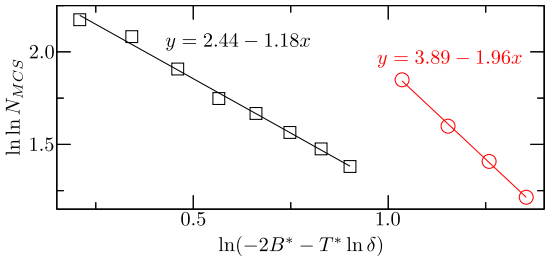

FIG. 4. Double logarithm of the average waiting time (in terms of Monte Carlo steps) versus the logarithm of the difference in volumetric free energy density between the two phases.

$N_{MCS} \propto t_w \propto I/I_0$ in the limit of long waiting times, and thus from classical nucleation theory we expect the plot of $\ln\ln N_{MCS}$ versus $\ln(-2B^* - T^* \ln\delta)$ to be a straight line with slope $1 - d$. Fig. 4 shows our simulation results meeting this expectation. Note that every average N_{MCS} was accumulated from one hundred independent simulations, each with a different random number seed and all sites initialised to the $+1$ state every time, and the waiting period was considered to be finished when the fraction of -1 sites has exceeded 0.5.

IV. MICROCANONICAL ENSEMBLE

A. Ray's approach to microcanonical Monte Carlo

As was already explained in Sec.I, it is both interesting and worthwhile to apply microcanonical sampling algorithms in studies of first-order phase transitions. Although all the equilibrium quantities can be inferred directly from the classical density of states, which can be computed efficiently by Wang-Landau sampling,[25] we will instead look to algorithms that admit kinetic simulations. There are (at least) two distinct approaches that suit our needs: one due to Creutz,[15,25] which Harris *et al.*[11,13] have used, and one due to Ray.[12,26] We adopt the latter, because it is simpler and more intuitive for atomistic systems.

Ray's approach to microcanonical MC relies on explicit assignment of conjugate momenta $\mathbf{p}$ and a kinetic energy $\mathcal{K}(\mathbf{p})$ to the Ising system. This assignment would be difficult to interpret for ferromagnetic systems, but it is natural for a system of classical particles. Now consider the uniform distribution in the classical N-particle phase space, subject to the constraint $\mathcal{H}(\boldsymbol{\sigma}, \mathbf{p}) = \mathcal{U}(\boldsymbol{\sigma}) + \mathcal{K}(\mathbf{p}) = E$:

$$\rho_E(\boldsymbol{\sigma}, \mathbf{p}) = C\delta_D(E - \mathcal{H}(\boldsymbol{\sigma}, \mathbf{p})), \tag{17}$$

where C is a normalisation constant (the inverse of the microcanonical partition function) and δ_D is the Dirac delta function. We would like to reduce (17) to a distribution over just the configuration space by integrating

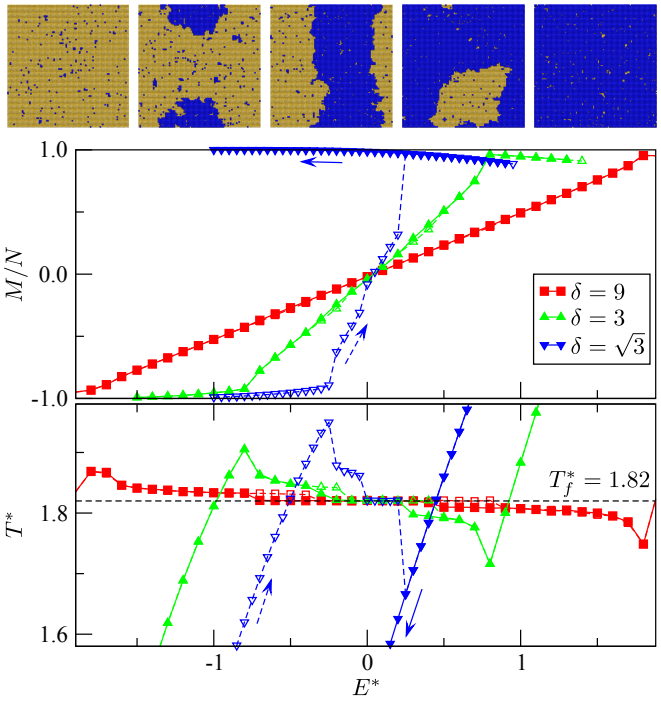

FIG. 5. Microcanonical caloric curves and magnetization plots calculated on 100×100 square lattice. The simulated system snapshots (top) are for $\delta = 3$, with solid (-1) sites in gold and liquid $(+1)$ sites in blue.

over the momentum dependence in the kinetic energy:

$$\rho'_E(\boldsymbol{\sigma}) = \int C\delta_D(E - \mathcal{H}(\boldsymbol{\sigma}, \mathbf{p}))\, d\mathbf{p}.$$

As explained by Pearson *et al.*,[27] the integration can be done by first taking a Laplace transform with respect to the energy

$$\mathcal{L}\{\rho_E(\boldsymbol{\sigma}\ \mathbf{p}; E)\}(s) = \int_0^\infty \rho_E(\boldsymbol{\sigma}, \mathbf{p}; E) e^{-sE}\, \mathrm{d}E.$$

This procedure separates the momentum coordinates, which can then be integrated over; inverting the transform then gives:

$$\begin{aligned} \rho'_E(\boldsymbol{\sigma}) &= C'(E - \mathcal{U}(\boldsymbol{\sigma}))^{dN/2-1} H(E - \mathcal{U}(\boldsymbol{\sigma})) \qquad (18) \\ &= \begin{cases} C'(E - \mathcal{U}(\boldsymbol{\sigma}))^{dN/2-1} & \text{if } \mathcal{U} \le E, \\ 0 & \text{otherwise,} \end{cases} \end{aligned}$$

where H denotes the Heaviside (i.e. unit step) function and d is the dimensionality. Replacing ρ_T in (14) by ρ'_E gives the appropriate rates for evolving Harris's degenerate Ising model consistent with Ray's microcanonical MC.

B. Simulations on square lattice (2D)

Equilibrium caloric curves and magnetization plots for a 100×100 square lattice are shown in Fig.5. The plots

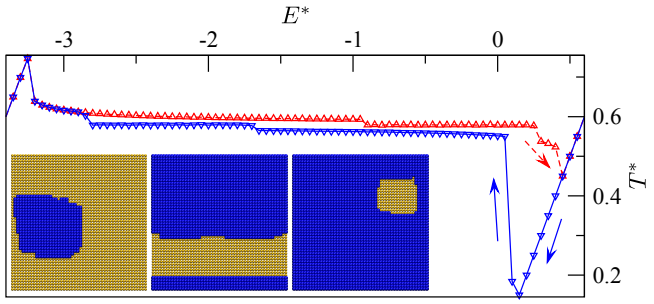

FIG. 6. Caloric curves and snapshots for 50×50 square lattice with $B^* = -2$ and $\delta = 1000$.

were generated by ramping the total dimensionless energy per site (E^*) up and down in increments of 0.1 or smaller, starting from the ground state, with the same number of MC steps used for equilibration and averaging as in Sec. II. The value of $T_f^* = 1.82$ was kept fixed, and three different sets of δ and B^* were chosen in accordance with (13). Note that increasing B^* and δ widens the coexistence range, consistent with the increase in latent heat. Also note how the data-points in the coexistence region do not rise monotonically with energy, but rather exhibit an overall downward slope. Such back bending in a caloric curve indicates negative heat capacity: the temperature of the system *decreases* as the total energy *increases*. The data points also exhibit distinct temperature jumps, whose magnitude decreases as δ and B^* increase. The origin of these jumps can be linked to topological changes in the phase boundary, resulting from finite size effects and periodic boundary conditions. From the instantaneous configuration snapshots we infer that the first jump corresponds to the nucleation of a quasi-circular liquid fraction in a solid; after the second jump the system forms a liquid band and a solid band with two quasi-planar interfaces; the next jump marks the break-up of the solid band, resulting in a quasi-circular solid fraction surrounded by the liquid; and after the last jump the system is completely molten. Not all the datasets have all four jumps: the state with a quasi-circular solid fraction does not occur for $\delta = \sqrt{3}$, and in that particular case the system also fails to solidify when the energy is ramped back down. This is again consistent with smaller B^* and δ making phase nucleation more difficult, as already discussed in Sec. III B.

Note that, although the topological transitions are ultimately an artefact of periodic boundaries, they have been recognised as a potential route for estimating the interface free energies in a variety of two-phase systems.[28–30] They have been analysed for equilibrium liquid-vapour interfaces simulated using the Lennard-Jones,[28,31] the q-state Potts,[30] and the lattice gas[29] models, all with periodic boundary conditions. However, we stress that the degenerate Ising model is distinctly different in that it is a two-state lattice model with variable bipartition of particles. The underlying microscopic mechanism differs from that of a conventional lattice gas: here the in-

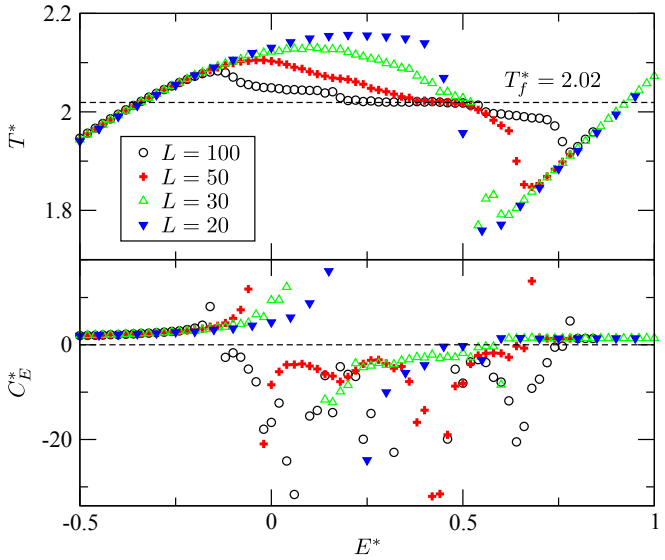

FIG. 7. Microcanonical caloric curves (top) and heat capacity plots (bottom) for the degenerate Ising model with $B^* = -0.7$ and $\delta = 2$ on square lattices of different size (L^2). Note that some values of C^*_E are outside the plotted range, intended for clearer illustration of $C^*_E < 0$ varying smoothly with E^* in certain regions of the coexistence range.

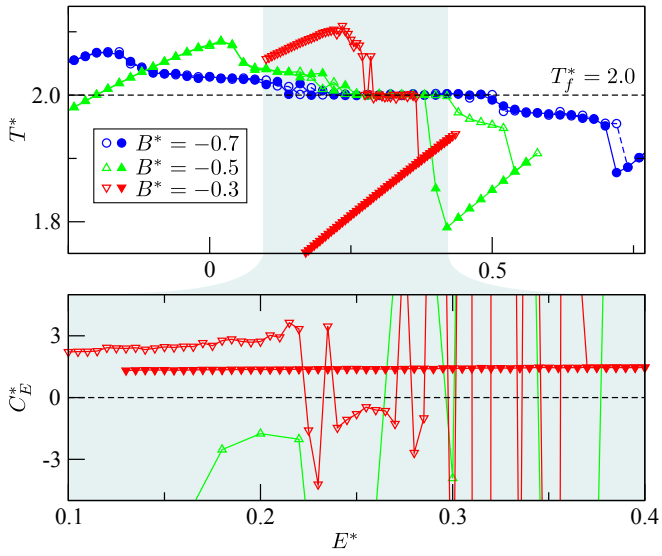

FIG. 8. Analogous to Fig.7, but the system size is kept fixed at 100×100 and the value of B is varied instead. Unfilled symbols correspond to heating, and filled symbols correspond to cooling.

terface topology changes solely *via* individual spin-flips, representing individual atoms changing phase; whereas conventional lattice-gas models rely completely on spin-exchanges, which correspond conceptually to the process of diffusive mass transport.

The snapshots of the phase boundary in Fig. 5 exhibit significant roughness and noticeable intermixing between the two phases. These characteristics are perhaps more reminiscent of the liquid-vapour interface, and they are due to our choice of relatively high T^*_f. In Fig. 6 we consider a lower value of $T^*_f = 0.58$ and find much sharper phase boundaries with planar facets. Note that we use a smaller (50×50) system in Fig. 6 to make microscopic features more apparent. Our results indicate that lowering $T_f (< T_c)$ generally reduces the degree of mixing between the two phases and yields a sharper phase boundary. This is where the degenerate Ising model is particularly useful, because it admits arbitrary tuning of the entropic barrier associated with nucleating a faceted phase boundary through adjustment of B^* and δ at fixed T^*_f, thus not interfering with the equilibrium structure of the interface (see Sec. III B).

C. Negative specific heat capacities

The inherent simplicity of the degenerate Ising model makes it straightforward to isolate the origin of negative specific heat capacities (C_E) in the microcanonical ensemble. Note that Chomaz *et al.*[32] have previously used a conventional lattice-gas model to analyse this phenomenon, and their microcanonical results were obtained by sorting *canonical* events generated with standard Metropolis MC sampling. The degenerate Ising model considered here is more general, and since we are operating within the microcanonical ensemble, we can calculate the heat capacity directly from the fluctuations in the kinetic energy by using[12,27]

$$C_E = Nk_B \left[N - (N - 2/d) \langle \mathcal{K} \rangle \langle \mathcal{K}^{-1} \rangle \right]^{-1}, \qquad (19)$$

where $\langle \dots \rangle$ indicates the (microcanonical) ensemble average of the quantity within, and $\mathcal{K}$ is the instantaneous kinetic energy.

In Fig. 7 we plot caloric curves and the corresponding $C^*_E \equiv C_E/Nk_B$ for systems of different size. It is immediately apparent that the back-bending in the caloric curves correlates with negative values of C^*_E. It is particularly noteworthy that C^*_E is negative and well-behaved (i.e. varies smoothly with E^*) only in parts of the coexistence region where the caloric curves are smooth and have negative (non-zero) slope. These particular patches correspond to crystal-melt interface topologies with non-zero mean curvature, in which case the interface-area-to-volume ration is ought to vary smoothly with E^* as the interface grows or shrinks. Whenever the two phases are separated by two disjointed crystal-melt interfaces with zero mean curvature (i.e. the banded topology in Figs. 5 and 6), the interface-area-to-volume ratio does not change with E^*, and the apparent slope of the caloric curves is always close to zero. In these flat patches C^*_E fluctuations erratically between large positive and large negative values, which is consistent with $C_E = (\partial T/\partial E)^{-1}$ diverging for $\partial T/\partial E = 0$. On the basis of these observations, we conclude that a necessary requirement for a smooth negative branch in heat capac-

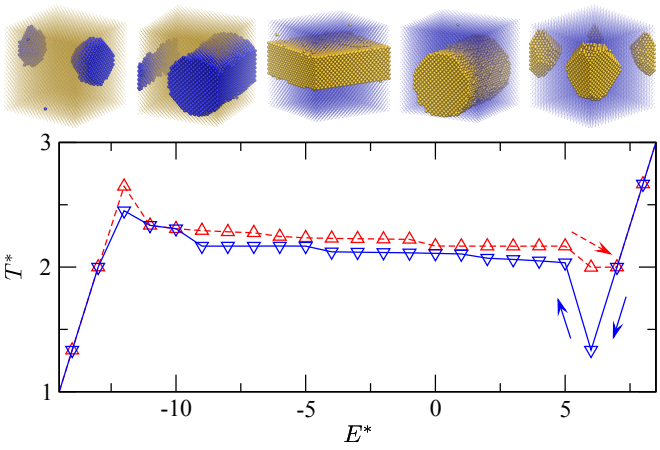

FIG. 9. Microcanonical caloric curves and configuration snapshots from simulations with $B^* = -10$ and $\delta = 10^4$ on fcc lattice with 32000 sites. The snapshots illustrate topological changes in the phase boundary at different energies in the coexistence range. Note that "liquid" sites are coloured blue and "solid" sites are in gold, and atomic radii are varied to aid visualisation.

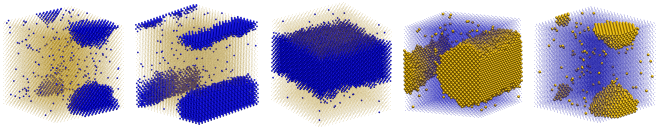

FIG. 10. Snapshots from simulations with $B^* = -9$ and $\delta = 64$, exhibiting a rougher phase boundary than in Fig. 9.

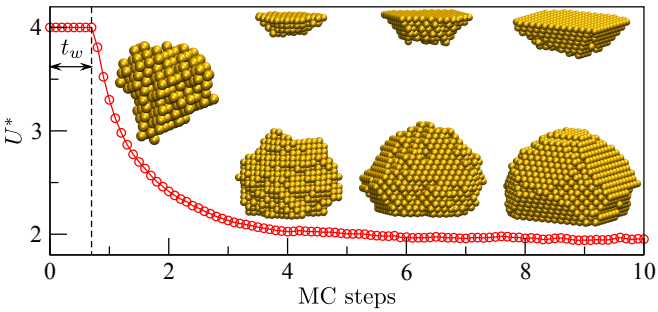

FIG. 11. Nucleation, growth and relaxation of a crystal from the melt (not shown) with $B^* = -10$, $\delta = 10^4$ and $E^* = 5$. One MC step is 32000 spin flips.

ity is that the interface-area-to-volume ratio must vary smoothly with the excitation energy.

It is clear from Fig. 7 that the negative C_E^* branch becomes less smooth as system size increases, consistent with the volumetric contribution dominating the total (communal) entropy and flattening the phase coexistence region. This observation suggests that smooth negative branches will vanish in the limit of infinite system size. However, within the degenerate Ising model it is also possible to manipulate the negative branches without varying system size, but rather by directly adjusting the communal entropy and the latent heat at fixed T_f, as demonstrated in Fig. 8.

D. Face-centred cubic lattice (3D)

We now move on to the three-dimensional face-centred cubic lattice, for which our canonical Metropolis MC yields $T_c^* \approx 9.8$, as expected.[33] Fig. 9 is analogous to Fig. 6, showing caloric curves obtained by first heating and then cooling a system of 32000 atoms on fcc lattice. Topological transitions occurring when the system passes through the coexistence region are also illustrated. For $T_f^* = 2.17$ the phase boundary is sharp and faceted, whereas increasing T_f^* leads to roughening of the interface and more intermixing between the two phases, as illustrated in Fig. 10 for $T_f^* = 4.33$.

E. Crystal nucleation and relaxation to a Wulff shape

The BKL algorithm[17] in principle allows us to study the kinetics as well as the equilibrium picture. In Fig. 11 we show results from simulated crystal nucleation, growth and subsequent relaxation to an equilibrium Wulff-like shape. The simulation was started from a fully liquid state and, after a waiting period of t_w (measured in terms of MC steps), a crystal eventually nucleates and rapidly expands. The growth slows due to the constant-energy constraint, and the crystal gradually relaxes to an equilibrium shape. Note how the interface structure is rough in the initial stages of rapid growth, but the overall shape remains close to spherical. Dendritic growth is not observed because the Mullins-Sekerka instability[34] is completely suppressed by the absence of thermal gradients in Ray's microcanonical MC. The present model effectively operates in the limit where heat transport occurs significantly faster than the propagation of phase boundaries. For more realistic modelling of far-from-equilibrium kinetics one can adopt Creutz's N-demon algorithm,[15,25] which is precisely what Harris *et al.* have used to simulate dendritic instabilities in two[13] and three[14] dimensions.

V. SUMMARY

We have revisited Harris's[11] degenerate Ising model and used it to simulate melting and crystallisation on square and face-centred cubic lattices. The model's distinguishing feature is a degeneracy parameter, representing the difference in communal entropy between the solid and the liquid phases, and it makes the field-driven first-order transition in the conventional Ising model occur at a precisely-defined temperature. We evolved the model by applying rejection-free canonical and microcanonical MC algorithms, with the microcanonical variant based

on the approach due to Ray.[12] We calculated canonical and microcanonical caloric curves and heat capacity plots, and we used this data to analyse the first-order phase transition when it is driven thermally. Particular attention was given to the equilibrium crystal-melt phase coexistence in the microcanonical ensemble. Our simulations show that the occurrence of negative specific heat capacities is more evident when a large portion of the total entropy is associated with the interface. We concluded that a necessary requirement for a smooth negative branch in a heat capacity plot is that the interface-area-to-volume ratio must vary smoothly with the excitation energy. Furthermore, a useful feature of the degenerate Ising model is that it allows for precise adjustment of bulk free energy differences completely independent of the interface free energy, which makes it possible to tune phase nucleation barriers at fixed degree of undercooling / overheating, without affecting the roughness of the interface. We exploited this feature to verify a dimension-dependent scaling expected from classical nucleation theory, providing additional evidence that this theory is valid in Ising-like lattice systems. Finally, we used the model to simulate crystal nucleation and subsequent relaxation to an equilibrium Wulff shape in the microcanonical ensemble, demonstrating the model's potential utility for simulation studies where detailed and accurate tracking of the phase boundary is a priority.

ACKNOWLEDGMENTS

This work was supported by the Royal Society of New Zealand Marsden Fund through contract number IRL0602, the MacDiarmid Institute for Advanced Materials and Nanotechnology, Fulbright New Zealand, and the US National Science Foundation through grant number DMS-1108643. The first author (DS) is grateful to Dr. Jacob Stevenson for helpful discussions related to this work.

[1] R. Wagner and W. Ellis, Appl. Phys. Lett. **4**, 89 (1964); J. S. Langer, Rev. Mod. Phys. **52**, 1 (1980); I. Weissbuch, L. Addadi, and L. Leiserowitz, Science **253**, 637 (1991); J. Chen, T. Herricks, M. Geissler, and Y. Xia, J. Am. Chem. Soc. **126**, 10854 (2004); A. Yethiraj, Soft Matter **3**, 1099 (2007); M. Wuttig and N. Yamada, Nature Materials **6**, 824 (2007).

[2] A. Karma and W.-J. Rappel, Phys. Rev. E **57**, 4323 (1998); K. R. Elder, N. Provatas, J. Berry, P. Stefanovic, and M. Grant, Phys. Rev. B **75**, 064107 (2007); S. van Teeffelen, R. Backofen, A. Voigt, and H. Löwen, Phys. Rev. E **79**, 051404 (2009).

[3] W. K. Burton, N. Cabrera, and F. C. Frank, Phil. Trans. R. Soc. A **243**, 299 (1951); G. H. Gilmer, Science **208**, 355 (1980); A. Pimpinelli and J. Villain, *Physics of crystal growth*, Vol. 53 (Cambridge university press Cambridge, 1998); J. D. Weeks and G. H. Gilmer, "Dynamics of crystal growth," in *Advances in Chemical Physics* (John Wiley & Sons, Inc., 2007) pp. 157–228.

[4] C. C. Battaile, D. J. Srolovitz, and J. E. Butler, J. Appl. Phys. **82**, 6293 (1997).

[5] N. Combe, P. Jensen, and A. Pimpinelli, Phys. Rev. Lett. **85**, 110 (2000).

[6] T. P. Schulze, Phys. Rev. E **78**, 020601 (2008).

[7] P. J. Steinhardt, D. R. Nelson, and M. Ronchetti, Phys. Rev. B **28**, 784 (1983).

[8] W. Lechner and C. Dellago, J. Chem. Phys. **129**, 114707 (2008).

[9] R. K. Pathria, *Statistical Mechanics*, 2nd ed. (Butterworth Heinemann, 1996).

[10] R. J. Baxter, *Exactly solved models in statistical mechanics* (Dover, 2007).

[11] R. Harris, Phys. Lett. A **111**, 299 (1985).

[12] Y.-L. Wang, F. Lee, and J. D. Kimel, Phys. Rev. B **36**, 8945 (1987); J. R. Ray and C. Freléchoz, Phys. Rev. E **53**, 3402 (1996).

[13] R. Harris, L. Jörgenson, and M. Grant, Phys. Rev. A **45**, 1024 (1992).

[14] L. Jörgenson, R. Harris, M. Grant, and H. Guo, Phys. Rev. E **47**, 1235 (1993).

[15] M. Creutz, Phys. Rev. Lett. **50**, 1411 (1983).

[16] N. Metropolis, A. W. Rosenbluth, M. N. Rosenbluth, A. H. Teller, and E. Teller, J. Chem. Phys. **21**, 1087 (1953).

[17] A. B. Bortz, M. H. Kalos, and J. L. Lebowitz, J. Comp. Phys. **17**, 10 (1975).

[18] T. D. Lee and C. N. Yang, Phys. Rev. **87**, 410 (1952).

[19] R. Griffiths, Physica **33**, 689 (1967).

[20] M. Blume, V. J. Emery, and R. B. Griffiths, Phys. Rev. A **4**, 1071 (1971).

[21] F. Y. Wu, Rev. Mod. Phys. **54**, 235 (1982).

[22] J. D. Stevenson, A. M. Walczak, R. W. Hall, and P. G. Wolynes, J. Chem. Phys. **129**, 194505 (2008).

[23] K. Binder and H. Müller-Krumbhaar, Phys. Rev. B **9**, 2328 (1974); T. Ray and J.-S. Wang, Physica A **167**, 580 (1990); P. A. Rikvold, H. Tomita, S. Miyashita, and S. W. Sides, Phys. Rev. E **49**, 5080 (1994); M. Acharyya and D. Stauffer, Eur. Phys. J. B **5**, 571 (1998); V. A. Shneidman, K. A. Jackson, and K. M. Beatty, J. Chem. Phys. **111**, 6932 (1999); S. Wonczak, R. Strey, and D. Stauffer, *ibid.* **113**, 1976 (2000); S. Ryu and W. Cai, Phys. Rev. E **81**, 030601 (2010).

[24] D. Turnbull and J. C. Fisher, J. Chem. Phys. **17**, 71 (1949); D. Turnbull, J. Appl. Phys. **21**, 1022 (1950).

[25] F. Wang and D. P. Landau, Phys. Rev. Lett. **86**, 2050 (2001); G. Bhanot, M. Creutz, and H. Neuberger, Nuclear Physics B **235**, 417 (1984).

[26] J. R. Ray, Phys. Rev. A **44**, 4061 (1991).

[27] E. M. Pearson, T. Halicioglu, and W. A. Tiller, Phys. Rev. A **32**, 3030 (1985).

[28] M. Schrader, P. Virnau, and K. Binder, Phys. Rev. E **79**, 061104 (2009).

[29] D. Winter, P. Virnau, and K. Binder, J. Phys.: Condens. Matter **21**, 464118 (2009).

[30] A. Tzöster and K. Binder, J. Phys.: Condens. Matter **24**, 284107 (2012).

[31] L. G. MacDowell, V. K. Shen, and J. R. Errington, J. Chem. Phys. **125**, 034705 (2006).

[32] P. Chomaz, V. Duflot, and F. Gulminelli, Phys. Rev. Lett. **85**, 3587 (2000).

[33] P. Lundow, K. Markstrm, and A. Rosengren, Philos. Mag. **89**, 2009 (2009).

[34] W. W. Mullins and R. F. Sekerka, J. Appl. Phys. **35**, 444 (1964).